PERGAMON

Chemical Engineering Science 56 (2001) 3517–3525

Chemical Engineering Science

www.elsevier.nl/locate/ces

Graded membrane supports produced by centrifugal casting of a slightly polydisperse suspension

P. Maarten Biesheuvel[a,*], Victor Breedveld[b], Arnoud P. Higler[c,1], Henk Verweij[a,2]

[a] *Department of Chemical Technology, University of Twente, P.O. Box 217, 7500 AE Enschede, Netherlands*
[b] *Department of Chemical Engineering, College of Engineering, University of California, Santa Barbara, CA 93106, USA*
[c] *Department of Chemical Engineering, Clarkson University, Potsdam, NY 13699, USA*

Received 10 February 2000; accepted 28 November 2000

Abstract

Tubular structures of a continuous particle size gradient are formed if a hollow cylindrical mold filled with a suspension of dispersed powder with a size distribution is centrifuged around its center axis. The mean particle size in the final structure increases gradually with increasing radial coordinate. Because the bulk properties can be optimized simultaneously with the surface composition, this process has advantages for the production of porous tubular ceramic membrane supports in case subsequent membrane layers are coated on the inner surface of the support. Particle velocities and concentrations in the suspension, as well as the compact profile, are numerically analyzed for completely filled molds. Using the analysis the composition at each location in the compact can be predicted, which can be used to calculate the permeance (flux per unit pressure difference), as well as the particle composition of the inner and outer surfaces.

Keywords: Sedimentation; Porous media; Multiphase flow; Membranes; Materials processing; Granular materials

1. Introduction

Porous ceramic membrane supports are often used as substrates for the subsequent deposition of a thin membrane with separative properties. The support provides mechanical stability (e.g., to withstand the pressure difference over the membrane) so that the thickness of the actual membrane can be minimized, resulting in a higher permeance (flux per unit pressure difference) (Biesheuvel & Verweij, 1999). The required thickness of the membrane is further limited by the smoothness of the support because the membrane material must cover all irregularities of the support to form a continuous, defect-free layer.

Ceramic membrane supports for gas- and liquid-phase separations are often cylindrical and not flat, because of several advantages in membrane modules:

- In general, a higher membrane surface area per unit of module volume.
- Flow profiles through tubes are better defined with less risk of dead zones.
- Better match to existing reactor concepts that are often based on tubular structures.

Cylindrical ceramic membrane supports produced by extrusion techniques are commercially available and applied in industrial separation units, but as these supports may have rather low surface smoothness (e.g. 6 μm) Nijmeijer, Huiskes, Sibelt, Kruidhof, and Verweij (1998) used centrifugal casting to produce cylindrical membrane supports from an electrostatically stabilized suspension of submicron α-alumina powder, which resulted in a support with a more homogeneous particle structure. The supports were sintered slightly to increase the handling strength while keeping the open porosity intact as much as

* Corresponding author. Current affiliation: Shell Global Solutions International B.V., Badhuisweg 3, 1031 CM Amsterdam, Netherlands. Tel.: +31-20-630-2349; fax: +31-20-630-3964.
E-mail address: maarten.p.m.biesheuvel@opc.shell.com (P. Maarten Biesheuvel).
[1] Current affiliation: Department of Chemical Technology, University of Twente, Netherlands.
[2] Current affiliation: Department of Materials Science and Engineering, The Ohio State University, Columbus, OH 43210, USA.

0009-2509/01/$ - see front matter
PII: S0009-2509(01)00037-9

possible. After sintering, supports were obtained with smooth inner (roughness $\sim$ 0.25 μm) and outer ($\sim$ 0.9 μm) surfaces.

Membranes can be coated on the inner or outer surface of these tubular supports. Advantages of application on the inner surface (compared to the outer surface) are as follows:

- After coating of the thin separative membrane onto the support, the membrane, by its sheer location, is better protected during the subsequent manufacturing steps of drying, sintering, machining and assembly in modules.
- The following reasoning suggests to locate the separative membrane layer at the feed side, and the feed side to coincide with the core of the tubes. To prevent accumulation in the support of components that are retained by the membrane, the separative membrane layer must be located directly at the high-pressure (feed) side. Else, permeance decreases significantly: simulations with the Dusty Gas Model showed that for a H_2/CH_4 mixture in a three-layer α-alumina/γ-alumina/silica system the permeance of hydrogen was significantly lower with the (selective) silica layer at the low-pressure (permeate) side (N.E. Benes, personal communication). This is especially true at high pressures because binary diffusion coefficients (e.g. of H_2/CH_4) are inversely proportional to pressure. At the feed side careful control of flow profiles is generally more critical than on the permeate side because fouling/cake layer formation occur at the feed side, and because a high selectivity (in membrane reactors) may require plug flow conditions. These demands are much better met within tubes than in the intermediary space between tubes.

Disadvantages of application on the inner surface (compared to the outer surface) are as follows:

- The lower surface area per unit module volume decreases the separation capacity. However, for a thin support (compared to the tube diameter) this effect is marginal.
- With the inside as high-pressure side (same side as membrane; see above) a tensile stress develops in the support instead of compressive stress. Ceramic materials withstand a compressive stress better than a tensile stress. However, the tensile strength of ceramics is often sufficient (dependent on tube radius and support thickness) to withstand pressures up to 50 bars (Biesheuvel & Verweij, 1999; Brinkman, Van Eijk, Meinema, & Terpstra, 1999) while such high pressures are not generally used due to high costs of compression and necessary safety measures.

In this paper, we discuss how centrifugal casting of dispersed particles results in a support ('compact') with a decreasing particle size from the outside to the inside of the tube. Such a support may combine small particles on the inner surface—high smoothness and suitable for subsequent membrane application on that surface—with large particles over the larger part of the support, resulting in a high permeance of the support when compared to a support consisting solely of the particles of the inner surface. From former work (Biesheuvel & Verweij, 2000; Biesheuvel, 2000) we know that in suspensions of repulsive particles (e.g., by electrostatic stabilization), particles of different size have different settling velocities resulting in a graded structure. A prerequisite is the presence of an external force that acts on the particles such as gravity or a centrifugal force.

The present paper is related to our former papers on centrifugal casting with suspensions of one particle type (Biesheuvel, Nijmeijer, & Verweij, 1998) and on centrifugal casting of suspensions containing two different particle types (Biesheuvel & Verweij, 2000). In the first a gradient in particle size over the support is not considered while the latter focuses on molds that are not completely filled, resulting (for two particle types) in the development of two distinct layers, instead of a smoothly graded support that develops in completely filled molds. In case of partial mold filling, modeling of systems of more than two particle types is very difficult, requiring the solutions of partial differential equations while taking care of the extreme sharp changes over the 'shocks' between different suspension phases. Only for dilute suspensions, e.g. at a volume concentration lower than 2%, somewhat simpler solutions can be derived since interparticle hydrodynamic interaction can be neglected. However, for a completely filled mold that rotates around its center axis, particle concentrations and velocities can be calculated from a set of ordinary differential equations only, due to the fact that the single initial suspension phase does not split up into several phases and concentration gradients do not develop because the particle flux is proportional to the radial coordinate (Biesheuvel, Nijmeijer, & Verweij, 1998; Biesheuvel & Verweij, 2000). Note that concentrations and composition of the suspension phase do change *in time*. The present paper is therefore focused on the phenomena occurring when the number of particle types increases from one or two to numbers that approximate a continuous size distribution (10–25).

To our knowledge, modeling the structure of a material formed from a powder with a particle size distribution has never been done before. Mathematical description of particle *motion* in a suspension of more than a few particle types (i.e., approximating a continuous size distribution) has been done for the case of gravity settling (Davis & Hassen, 1988; typically 25 particle types) but not for centrifugation. In the gravity case, distinct suspension phases always develop, in contrast to the case of a completely filled mold rotating around its center axis in which case—as discussed above—the suspension remains a single phase without composition gradients.

The fact that no concentration gradients develop in a completely filled cylindrical mold centrifuged around its center axis has an interesting consequence: after a certain period of centrifugation, we can take an arbitrary sample from the suspension (independent of location) and from this sample, which represents the entire suspension phase, we can determine the size distribution, for instance, by a light scattering technique (see Section 3). The fact that we do not need to know the exact location simplifies sampling enormously. In addition, we can take a large sample which is necessary when the suspension becomes dilute. Such an experiment is impossible for a mold that is not completely filled, for centrifugation around an axis perpendicular to the cylinder's center axis (uni-axial geometry) and under gravity settling. This simple and precise technique may be very useful to study the sedimentation behavior of concentrated, multicomponent suspensions of particles in the nanometer range. Another technique which we investigated was the analysis by scanning electron microscopy of a cross-section of a sintered support tube. However, resolution was too low to measure either a size distribution at a certain spot (radial coordinate) or a size gradient (change of particle size with radial coordinate).

In the present paper, we discuss, validate and evaluate a transport model that predicts the particle size distribution in a membrane support consolidated by centrifugal casting. Only a completely filled mold is considered which largely simplifies calculations and experiments, as discussed above.

2. Theoretical background

Particle velocities in multicomponent batch sedimenting systems are described by (Biesheuvel, Verweij, & Breedveld 2001)

$$U_i = U_{i0} h_i \frac{\rho_i - \rho_s}{\rho_i - \rho_0} - \sum_{j=1}^{m} U_{j0} h_j \frac{\rho_j - \rho_s}{\rho_j - \rho_0} \phi_j \tag{1}$$

with the particle velocity at infinite dilution, U_{i0}, given by Stokes' law

$$U_{i0} = \frac{d_i^2(\rho_i - \rho_0)}{18\eta} \omega^2 r \tag{2}$$

which is valid in laminar flow for spherical particles in the absence of wall effects. Here, m is the number of different species, i the species index, d_i is the particle diameter, ρ_i the particle density, ρ_0 the liquid density, ω the rotational velocity (rad/s), r the radial coordinate, η the Newtonian viscosity of the liquid and h_i the particle hindrance function that incorporates hydrodynamic particle interactions.

The suspension density ρ_s is given by

$$\rho_s = (1 - \phi_{\text{tot}})\rho_0 + \sum_{j=1}^{m} \phi_j \rho_j, \tag{3}$$

ϕ_{tot} being the total volumetric particle concentration in suspension

$$\phi_{\text{tot}} = \sum_{j=1}^{m} \phi_j. \tag{4}$$

State-of-the-art expressions for the hindrance function h_i are given by Patwardhan and Tien (1985) incorporating variations in local porosity around particles of different size

$$h_i = \left(1 - \left(1 + \frac{d_\varepsilon}{d_i}\right)^{-3}\right)^{n-2}, \qquad d_\varepsilon = \frac{\sum_{j=1}^{m} d_j \phi_j}{\phi_{\text{tot}}} (\phi_{\text{tot}}^{-1/3} - 1). \tag{5}$$

The power n depends on Reynolds number and particle size to vessel size ratio, but for laminar flow without wall effects, $n = 4.65$ (e.g., Biesheuvel, 2000; Biesheuvel, et al., 2000). When the local particle concentration $(1 + d_\varepsilon d_i^{-1})^{-3}$ (local at the particle scale) is set equal to the average suspension concentration ϕ_{tot} (averaged over a large ensemble of particles but dependent on the macroscopic radial coordinate r), (5) simplifies to (Masliyah, 1979)

$$h_i = (1 - \phi_{\text{tot}})^{n-2}. \tag{6}$$

Particle concentrations in suspension are given by a particle mass balance (equation of continuity for species i), which, for a one-dimensional cylindrical geometry, reads

$$\frac{\partial \phi_i}{\partial t} = -\frac{1}{r} \frac{\partial}{\partial r}(r \phi_i U_i). \tag{7}$$

Because all particles have the same density ρ, combination of (1), (2) and (7) results for an initially homogeneous suspension in

$$\frac{\partial \phi_i}{\partial t} = -\frac{\phi_i \omega^2 (\rho - \rho_0)}{9\eta} \times \left(d_i^2 h_i - \sum_{j=1}^{m} d_j^2 h_j \phi_j\right)(1 - \phi_{\text{tot}}) \tag{8}$$

with h_i given by (5). We refer to Biesheuvel et al. (1998), Biesheuvel and Verweij (2000) and references therein for a detailed account why gradients in particle concentration do not develop for an initially homogeneous suspension. With (6), (8) simplifies to

$$\frac{\partial \phi_i}{\partial t} = -\frac{\phi_i \omega^2 (\rho - \rho_0)}{9\eta} \left(d_i^2 - \sum_{j=1}^{m} d_j^2 \phi_j\right)(1 - \phi_{\text{tot}})^{n-1}. \tag{9}$$

Growth of the compact follows from a Kynch (1952) balance over the compact–suspension boundary ('front'). In its most general form (multicomponent suspension,

densification, infiltration by fines and kinematic waves all allowed for) it is given by

$$\sum_{j=1}^{m}(U_j - U_c)\phi_j = \sum_{j=1}^{m}(U_{c,j} - U_c)\phi_{c,j}. \quad (10)$$

Here, the particle velocity in suspension U_j is considered exactly at the compact front (r_c), while U_c is the velocity of the front, $U_{c,j}$ the velocity of particles within the compact at r_c and $\phi_{c,j}$ the volumetric concentration of particles in the compact at r_c. This form of the *Kynch* balance is relevant if different particles within the compact have different velocities, e.g., when the small particles trickle through the matrix structure of the larger particles (Civan, 1998; Hampton, Savage, & Drew, 1992). However, assuming that at the compact–suspension front all particles *in the compact* have the same velocity ($\forall j : U_{c,j} = U_{c,\mathrm{all}}$), (10) simplifies to

$$\sum_{j=1}^{m}(U_j - U_c)\phi_j = (U_{c,\mathrm{all}} - U_c)\phi_c, \quad \sum_{j=1}^{m}\phi_{c,j} = \phi_c. \quad (11)$$

The composition of the layer that deposits at a certain time can be derived from (11)

$$f_i = \frac{(U_i - U_c)\phi_i}{\sum_{j=1}^{m}(U_j - U_c)\phi_j}, \quad \sum_{i=1}^{m} f_i = 1. \quad (12)$$

Here, f_i is the fraction of particle type i. Biesheuvel and Verweij (2000) already derive (12), but on the basis of an incompressible material (i.e., Eq. (13)). That the equation for f_i also holds for a compressible compact (thus under conditions of densification, $U_{c,\mathrm{all}} \neq 0$) can be understood by the fact that during densification particles in a given plane remain within that plane, so that even though the total concentration ϕ_c may increase, the fractions f_i remain the same.

To solve Eqs. (11) and (12), information is needed on the change in time of the compact concentration ϕ_c, suspension concentrations ϕ_i and particle velocities at both sides of the suspension–compact front $U_{c,\mathrm{all}}$ and U_i. From this point forward, we assume that the suspension and the compact are separated by a kinematic shock (Biesheuvel et al., 1998). Therefore, ϕ_i and U_i follow from solution of the continuity equations for the bulk of the suspension, (1) and (8). We further assume zero compact densification ($U_{c,\mathrm{all}} = 0$). Therefore, (11) simplifies to

$$\sum_{j=1}^{m}(U_j - U_c)\phi_j = -U_c\phi_c. \quad (13)$$

After rewriting, (13) results in

$$\frac{\mathrm{d}r_c}{\mathrm{d}t} = U_c = -\frac{\sum_{j=1}^{m} U_j\phi_j}{\phi_c - \phi_{\mathrm{tot}}}. \quad (14)$$

In this work we will use a constant ϕ_c—independent of the particle size distribution function—for reasons of simplicity. For a two-component compact of spherical particles Biesheuvel (2000) uses the Westman–Hugill equations while we refer to Yu and Standish (1987) for expressions for the packing factor of a sediment consisting of spherical particles with a size distribution. As long as the expression for ϕ_c in terms of particle fractions and sizes is explicit, the numerical scheme does not essentially become more complicated.

3. Materials and methods

Experiments were performed with a 20 vol% suspension of α-alumina powder (AKP-15, Sumitomo, Tokyo, Japan) in water stabilized with nitric acid at a concentration of 0.02 M HNO_3. The powder has a volume average size d_{av} of $\sim$ 750 nm with $>90\%$ within the range 500–1100 nm. The suspension is ready for use after ultrasonic treatment to obtain optimum particle dispersion and filtration over a 200 μm filter to remove agglomerates (Biesheuvel & Verweij, 1999). Note that the AKP-powder series have a very sharp particle size distribution compared to other commercially available alumina powders in that size range. Therefore, the effects that we measured with AKP-15 will probably be even more pronounced for many other ceramic submicron powders.

Centrifugation is done in the same home-made centrifuge as used in Nijmeijer et al. (1998) and Biesheuvel et al. (1998). The cylindrical metal molds (length 6–10 cm; internal diameter 2 cm) are filled completely with suspension and stoppered on both ends using Teflon caps with rubber rings. After mounting in the centrifuge, the rotational velocity (of the steel molds around their center axis) is increased in $\sim$ 10 s to 3500 rotations per minute ($\omega = 367$ rad/s). After 2.5, 5, 7.5 or 10 min, the velocity is decreased again in $\sim$ 10 s. These periods are short compared to the actual process time (2×10 s on 150 s (=13%) is the largest error made). Note that as particle velocities scale with ω^2, the influence of the periods of start-up and deceleration on compact formation is actually well below 13%, see Eq. (2). Moreover, we assume that deceleration was sufficiently slow ($\sim$ 37 rad/s^2) to avoid redispersion of particles that were already deposited (Biesheuvel et al., 1998).

After centrifugation for a certain time, the mold was opened and part of the suspension pipetted from the inner core of the mold and transferred into the recycle loop of an optical size analyzer (Microtrac X-100, Leeds and Northrup, North Wales, PA, USA) to determine the composition of the suspension. Centrifugation was not continued but suspension and formed compact were removed. A new centrifugation run always started with fresh suspension. For centrifugation of 5 min and more the suspension was very dilute—most particles had already deposited—and a large percentage (up to 50–75%) of the suspension volume in the mold had to be used to obtain a sufficient

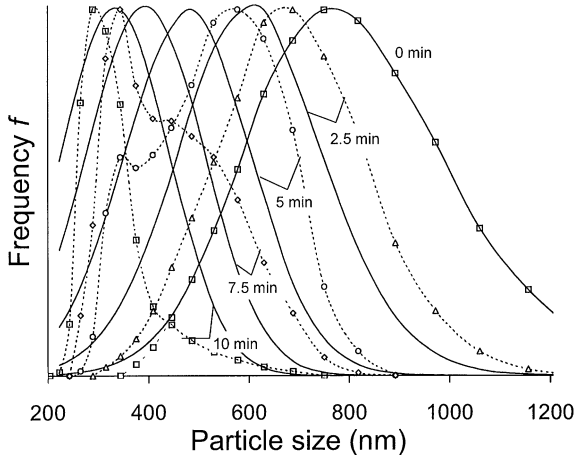

Fig. 1. Suspension composition. Comparison of experimental results (dots connected with dashed lines) with model predictions (solid lines) for 2.5, 5, 7.5 and 10 min after start of rotation (0 min).

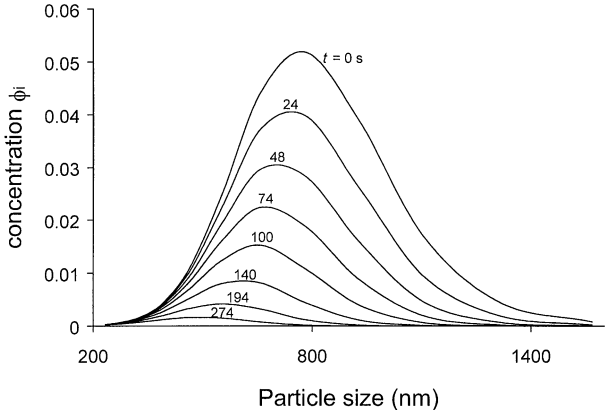

Fig. 2. Simulated suspension concentration as function of time and particle size. The upper right curve is the initial composition. The mode of the curve shift to smaller sizes while the total suspension concentration ϕ_{tot} decreases sharply in time. Numbers give the time in seconds.

particle concentration in the recycle loop of the size analyzer.

Numerical calculations on particle concentration and velocity in the suspension, the compact front velocity U_c and its composition f_i follow from solution of the ordinary differential equations (8)/(9) and (14) and the algebraic equations (4), (5) and (12). The initial conditions are

$$t = 0 : r_c = r_m, \phi_i = \phi_{i,0}.$$

This set of differential and algebraic equations is solved numerically with a third order semi-implicit Runge–Kutta scheme combined with a Bulirsch–Stoer extrapolation method for step size adjustment. Calculations were done with the *BESIRK*-subroutine of Maple, a computer algebra system (Schwalbe, Kooijman, & Taylor, 1996).

4. Results

4.1. Suspension

The experiments as discussed in the former section are compared with simulation results in Fig. 1. Simulation results using Eq. (9) are presented here, but results based on Eq. (8) are very similar: only for 2.5 min the maximum of the distribution is shifted somewhat to higher sizes (~ 20 nm) for Eq. (8), while for larger times no difference can be observed because the suspension is very diluted and the hindrance factors approach unity, irrespective of the hindrance function used. Data used in the simulations are $\omega = 367$ rad/s, $\eta = 1$ mPa s, $\rho = 3970$ kg/m^3, $\rho_0 = 1000$ kg/m^3, n=4.65, m=24, r_m=10 mm and ϕ_c=0.55.

The initial, measured size distribution was used as input in the model except for size fractions of 446 nm and smaller. This part of the distribution was replaced by a Gaussian distribution obtained by fitting part of the original distribution (particle size 446 to 750 nm) with $f = \sigma^{-1}(2\pi)^{-1/2} \exp(-\frac{1}{2}((d - d_{\text{av}})/\sigma)^2)$ (f being the frequency or differential mass; $d_{\text{av}} = 750$ nm, $\sigma = 160$ nm) and extrapolating this equation to sizes below 446 nm. We have chosen this procedure because the measured initial fraction for sizes of 344 nm and smaller is zero, which is erroneous because these particle types are detected in the suspension after 7.5 and 10 min of centrifugation, when the larger particles have deposited. The small particles are not measured in the initial suspension because their concentration is below the detector threshold.

With this modification of the initial conditions we find a comparison that—though clearly not of the quality we would have wished—is satisfactorily at this point in the analysis. The deviation of model and experiment can partly be attributed to the experimental difficulties in determining the small particle tail of the initial size distribution. Also, a bimodal distribution with the small particle peak between 330 and 360 nm was observed after 5 and 7.5 min of centrifugation, which shows that the initial suspension (powder) contained a fraction of 'fines' of this size, unobserved in the analysis of the original powder.

Further simulations are made based on Eq. (9) but with the 24 fractions of Fig. 1 reduced to $m = 12$ fractions by grouping (d_i, ϕ_i)-pairs, which results in $d_1 = 1567$ nm, $d_2 = 1318$ nm, $d_3 = 1108$ nm, $d_4 = 932$ nm, $d_5 = 784$ nm, $d_6 = 659$ nm, $d_7 = 554$ nm, $d_8 = 466$ nm, d_9=392 nm, d_{10}=329.5 nm, d_{11}=277 nm, d_{12}=233 nm, $\phi_{1,0} = 0.00802$, $\phi_{2,0} = 0.0436$, $\phi_{3,0} = 0.0167$, $\phi_{4,0} = 0.0385$, $\phi_{5,0} = 0.0518$, $\phi_{6,0} = 0.0443$, $\phi_{7,0} = 0.0252$, $\phi_{8,0} = 0.0112$, $\phi_{9,0} = 0.00440$, $\phi_{10,0} = 0.00170$, $\phi_{11,0} = 0.000680$, $\phi_{12,0} = 0.000289$.

Fig. 2 shows that the mode of the particle size distribution in the suspension shifts to lower sizes in time while the total particle concentration ϕ_{tot} (given by

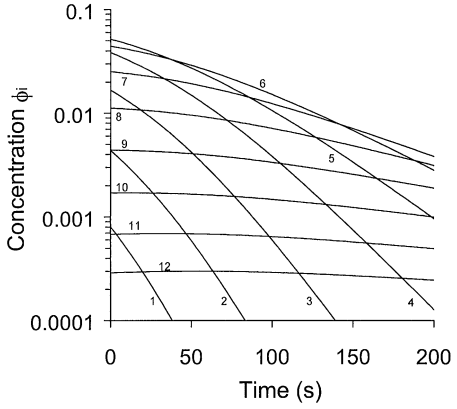

Fig. 3. Concentrations in suspension for the 12 particle species. The concentration of particles increases initially for the smaller particle types 10, 11 and 12. The larger the particle, the faster the concentration decreases in time.

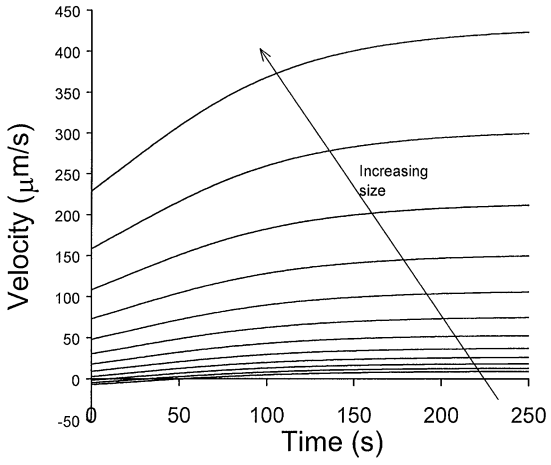

Fig. 4. Particle velocities in suspension at the suspension–compact front r_c (r_c decreases in time from r_m to $r_{c,\infty}$). Note that the maxima in Fig. 3 (for particle species 10–12) coincide exactly with the time at which particle velocities are zero in Fig. 4.

$(d_m - d_1)^{-1} \int_{d_1}^{d_m} \phi_i \, \mathrm{d}d$) decreases in time. Several features are more clearly depicted in Fig. 3, such as the fact that the concentration of the three smallest particle species (10–12) initially *increases*. The rate of concentration decrease (with time) increases with particle size ($\mathrm{d}/\mathrm{d}d_i \, |\mathrm{d}\phi_i/\mathrm{d}t| > 0$).

Particle velocities at the compact front r_c are shown in Fig. 4. Initially, velocities are negative for the three smallest species because their slip velocity with the liquid is low and large particles moving outward displace the liquid and these small particles (the liquid velocity is always and everywhere negative, thus pointing inward). As a result, for the small particle types the volume concentration in the suspension phase initially increases. Particle velocities increase with time because ϕ_{tot} decreases and the particle hindrance function h_i *increases*, see Eq. (1).

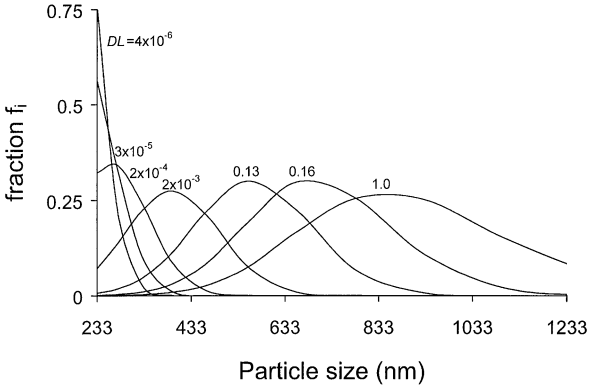

Fig. 5. Particle size distribution for several values of the dimensionless location DL (DL = 0 being the inside of the compact at $r_{c,\infty} = 8.0$ mm and DL = 1 the outside at $r_m = 10$ mm).

Because r_c decreases in time (starting at $r_m = 10.0$ mm, while $r_{c,\infty} = 8.0$ mm) and particle velocities are proportional to r the particle velocity for a certain species i at a certain coordinate r^* increases faster than depicted in Fig. 4.

4.2. Compact

The simulations also reveal interesting features about the compact profile. Fig. 5 shows the change of size distribution with dimensionless location in the compact $\mathrm{DL} = (r_c - r_{c,\infty})(r_m - r_{c,\infty})^{-1}$. Compact formation starts at $r_c = r_m$ (outer layer, DL = 1) and ends when the last particles deposit at $r_c = r_{c,\infty}$ (inner layer, DL = 0). The particle size distribution in the compact at DL = 1 is skewed toward larger particles compared to the (initial) suspension distribution from which it is formed (upper right curve in Fig. 2). All particles are present in the first layers formed. Subsequently, deposited layers are enriched in small particles: the mode moves to a lower size. Furthermore, the distribution function sharpens with decreasing DL. Fig. 6 shows the fraction of each species as function of location. The fraction of large particles decreases in time (with decreasing DL): e.g. for DL < 0.1, the fraction of particle species 3 has virtually become zero. In time (with decreasing DL) more and more sizes experience this destiny and finally (last layer at DL = 0) only the smallest size remains at a fraction of unity ($f_1 = 1$).

The continuum approach fails when significant gradients exist at the scale of the particle. For a typical smallest particle size of 200 nm and a final compact thickness of 2 mm, this implies that all predictions in Figs. 5 and 6 for $\mathrm{DL} < 1 \times 10^{-4}$ must be discarded. Thus, the composition of the final inner layer is best approximated—in this case—by the distribution at $\mathrm{DL} = 1 \times 10^{-4}$. However, in other simulations (not reported) based on a higher initial concentration of smallest particles, the final compact layer consisted of the smallest particle species only.

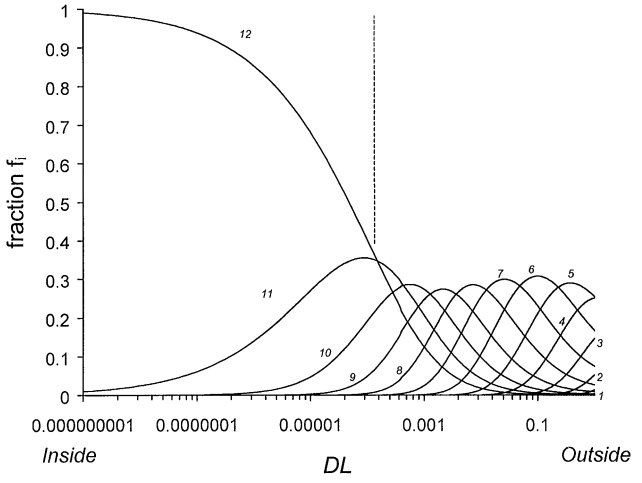

Fig. 6. Composition of the final compact as function of dimensionless location. The dashed line shows the lower limit of applicability of the continuum equations.

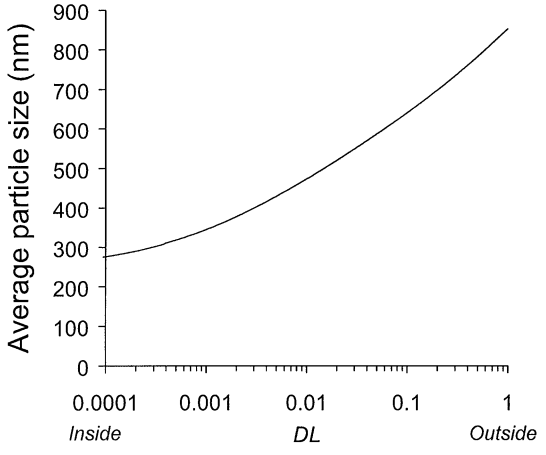

Fig. 7. Average particle size as function of dimensionless location.

The data in Fig. 6 are summarized in Fig. 7 using an average particle size given by

$$d_{\mathrm{av}} = \sum_{j=1}^{m} \phi_j d_j. \tag{15}$$

The inside and outside average sizes are now calculated as 280 nm ($\mathrm{DL} = 1 \times 10^{-4}$) and 850 nm ($\mathrm{DL} = 1$) which are in excellent agreement with the surface roughness measured by Nijmeijer et al. (1998), 250 and 900 nm.

4.3. Permeance

Simulations as performed above may be of help in the optimization of membrane supports by determining the optimum powder types (size and size distribution of powder types) and the concentrations of the different powders used (i.e., blending). For a support on which membranes are coated on the inner surface, one would like to optimize simultaneously the permeance of the support and the smoothness of the inner surface. The total powder concentration ϕ_{tot} results in a certain support thickness while the powder blending results in the gradients of the average particle size and the packing factor. A full-fledged optimization scheme would also incorporate a mechanical treatment including strength, stress and safety factors (Biesheuvel & Verweij, 1999).

In the following, we make a very simple first-order calculation in which we compare the permeance of the graded tube discussed above with a tube consisting of a monomodal particle size of 280 nm which is the average particle size of the inner surface of the graded tube. We make this calculation to show *how* such calculations can be performed; we will not perform an actual optimization. As objective function, we choose the volumetric permeance Π of the system in m^3 of permeate per m^2 of cross-sectional surface per Pa pressure difference per second (m/Pa s). We make simulations for a constant density (i.e., liquid) and a cylindrical geometry. This geometry requires that the cross-sectional surface is defined, for which we choose the inner surface $2\pi r_{c,\infty} L$ with L the length of a tube.

Note that because during subsequent sintering the support typically densifies (increasing ϕ_c) and the thickness ($r_m - r_{c,\infty}$) decreases, simulation results should ideally be rescaled to the sintered thickness. However, in the next calculation we assume that ϕ_c remains constant during sintering. This assumption is underpinned by experiments in our laboratory (Nijmeijer et al., 1998) which show that centrifuged tubes do not shrink much ($\sim 5\%$) during sintering at 1150°C and 1 h (the outer diameter r_m decreases $\sim$0.5mm from $r_m = 10$ mm in the compact after centrifugation). The volumetric permeance follows from Darcy's law

$$J_{\mathrm{vol}} = -k\eta^{-1}\nabla P, \tag{16}$$

with k being the permeability (m^2) and ∇P the pressure gradient (Pa/m). In (16) only a pressure gradient is implemented as driving force (Biesheuvel & Verweij, 1999) and the equation only considers viscous flow of a Newtonian fluidum (Benes, Biesheuvel, & Verweij, 1999).

Combination of (16) with the equation of continuity results for stationary flow in

$$\Pi = \frac{\Phi}{2\pi r_{c,\infty} L \Delta P} = \left(r_{c,\infty}\eta \int_{r_{c,\infty}}^{r_m} \frac{1}{rk}\,\mathrm{d}r \right)^{-1}. \tag{17}$$

Here, Φ is the total volume flow (m^3/s) through the cylinder wall. We use a modified Carman–Kozeny expression for the permeability of a multicomponent structure—a procedure discussed by Philipse (1997)—which results in (see also Biesheuvel, 2000)

$$k = \frac{(1-\phi_c)^3}{180\phi_c^2} \left(\sum_{j=1}^{m} \frac{f_j}{d_j} \right)^{-2}. \tag{18}$$

For simplicity, we assume a constant packing factor ϕ_c in the following calculation and we again refer to Yu and Standish (1987) for a description of ϕ_c as function of the particle size distribution function. For an ideal monocomponent powder (one particle species of a single size) a homogeneous compact is obtained for which combination of (17) and (18) results in

$$\Pi = \frac{(1-\phi_c)^3 d^2}{180 r_{c,\infty}\eta\phi_c^2 \ln(r_m/r_{c,\infty})}. \tag{19}$$

With $\phi_c = 0.55$, $r_{c,\infty} = 7.977$ mm, $\eta = 1$ mPa s, $r_m = 10$ mm and $d = 280$ nm, Eq. (19) results in $\Pi = 7.28 \times 10^{-11}$ m/Pa s. For our graded support, we numerically solve for Π using the data associated with Figs. 5 and 6: for n values of r (with r_ℓ ranging from $r_1 = r_{c,\infty}$ to r_m) we have values for the fractions f_j (j from 1 to m) for each particle size d_j. In summation form, Π is then given by

$$\Pi = \frac{(1-\phi_c)^3}{180 r_{c,\infty}\eta\phi_c^2} \left\{ \sum_{\ell=1}^{n} \left\{ \frac{(r_\ell - r_{\ell-1})}{r_\ell} \left(\sum_{j=1}^{m} \frac{f_j}{d_j} \right)^2 \right\} \right\}^{-1}. \tag{20}$$

which gives (for $m = 12$) as numerical result $\Pi = 4.38 \times 10^{-10}$ m/Pa s. This value is 6 times higher than for a monocomponent compact with $d = 280$ nm which means a significant improvement in permeance while the inner surface smoothness remains the same.

5. Discussion

The present work is an exploratory study. Several lines of research can be thought of to refine and extend its conclusions:

- Development of a mechanical treatment for graded structures—analoguous to the one in Biesheuvel and Verweij (1999) for materials without size or porosity gradients—which takes account of the strength as a function of the particle size distribution (and packing factor). The weakest link must be identified (i.e. the radial coordinate of minimum strength/stress ratio).
- Full-fledged optimization based on simulations with real powder blends (several powders, each with a size distribution) including the mechanical aspects. In general, we can expect that mixing a suspension of large particles with a small amount of small particles will result in a tube with a high permeance and a smooth inner surface (Darcovich & Cloutier, 1999). Disadvantages of the use of such a binary suspension are the possibility of small particles trickling through the already formed matrix of larger particles, and fracture during sintering due to the sintering stresses induced at the abrupt particle size change in the compact near the inner surface. These disadvantages may be overcome by using a partly overlapping size distribution of the small and the large particle fraction, while particle trickling is easily overcome because for trickling to occur through a bed of touching spheres the particle size ratio (of spheres) must at least be 6.5:1.
- Better experimental methods based on an open, and larger, centrifuge (see references in Biesheuvel et al., 1998) allow continuous and in situ sampling.
- Centrifugation of a blend of two distinct powders will give better validation of the transport models (compared to the present validation based on a single powder with a size distribution) because in that case the difficult problem of exactly determining the particle concentration in the small-particle tail of the initial powder sample is circumvented.

6. Conclusions

Centrifugal casting of particles with a size distribution results in a structure with increasing average particle size with radial coordinate. In contrast to more outward layers, that contain all particle types, the final deposition layer in some cases only consists of the smallest particle type. The predicted average particle size of the inside and outside of a tube produced from a submicron alumina powder agrees well with surface roughness measurements from literature. The formation of the compact is accompanied by a decrease in average size of the suspended particles, which can be monitored by sampling the suspension and analyzing the particle size distribution with a laser technique.

Simulations are in qualitative agreement with experiments. Both show that the particle concentration decreases with time and decreases fastest for the largest particles; therefore in time the average particle size in the suspension decreases. During the first moments of the experiment, the smallest particles in the suspension have a settling velocity pointing *inward* while the suspension concentration of these particles *increases*. Only after the largest particles have moved out of suspension, the direction of velocity of the small particles changes sign and they move outward, so that their concentration starts to decrease as well.

The permeance (volume flux per unit pressure difference) of these graded supports is much higher than of supports consisting only of the small particles of the inner surface. Thus, segregation effects in the centrifugation of a powder with a size distribution are advantageous for the design of membrane systems in case subsequent membranes will be deposited on the inner surface of the tubular support.

Notation

d_i	particle size, m
DL	dimensionless location in compact, $=(r_c - r_{c,\infty})(r_m - r_{c,\infty})^{-1}$, dimensionless
f_i	local fraction of particle type i in compact, dimensionless
h_i	particle hindrance function in suspension, dimensionless
L	tube length, m
m	number of different particle types
n	hindrance factor power, dimensionless
P	pressure, Pa
r	tube coordinate (distance from heart of tube), m
r_c	location of suspension–compact front, m
$r_{c,\infty}$	coordinate of inner surface of final compact, m
r_m	inner diameter of mold. Outside of compact, m
t	time, s
U_c	growth velocity of compact = velocity of suspension–compact front, m/s
$U_{c,i}$	velocity of particle species i within the compact at r_c, m/s
$U_{c,\mathrm{all}}$	velocity of all the particle species within the compact at r_c, m/s
U_i	velocity of particle type i in suspension, m/s
U_{i0}	settling velocity at infinite dilution, m/s

Greek letters

ε	compact porosity, dimensionless
η	liquid Newtonian viscosity, Pa · s
Π	permeance, m/(Pa · s)
ρ_0	density of liquid, kg/m^3
ρ	density of particles, kg/m^3
ρ_s	suspension density, kg/m^3
ϕ_c	compact packing factor (unity minus porosity ε), dimensionless
$\phi_{c,i}$	volumetric concentration of particle species i within the compact at r_c, dimensionless
ϕ_i	volumetric concentration of type i in suspension, dimensionless
ϕ_{tot}	total volumetric concentration of particles in suspension, dimensionless
ω	rotational velocity, rad/s

Acknowledgements

We thank Arian Nijmeijer, Cindy Huiskes and Natascha Sibelt for their help with the experiments and Niels Peters for his suggestion to measure the suspension composition.

References

Benes, N. E., Biesheuvel, P. M., & Verweij, H. (1999). Tensile stress in a porous medium due to gas expansion. *A.I.Ch.E. Journal*, *45*, 1322–1328.

Biesheuvel, P. M. (2000). Particle segregation during pressure filtration for cast formation. *Chemical Engineering Science*, *55*, 2595–2606.

Biesheuvel, P. M., Nijmeijer, A., & Verweij, H. (1998). Theory of batchwise centrifugal casting. *A.I.Ch.E. Journal*, *44*, 1914–1922.

Biesheuvel, P. M., & Verweij, H. (1999). Design of ceramic membrane supports: permeability, tensile strength and stress. *Journal of Membrane Science*, *156*, 141–152.

Biesheuvel, P. M., & Verweij, H. (2000). Calculation of the composition profile of a functionally graded material produced by centrifugal casting. *Journal of the American Ceramic Society*, *83*, 743–749.

Biesheuvel, P. M., Verweij, H., & Breedveld, V. (2001). Evaluation of instability criterion for bidisperse sedimentation. *A.I.Ch.E. Journal*, *47*, 45–52.

Brinkman, H. W., Van Eijk, J. P. G. M., Meinema, H. A., & Terpstra, R. A. (1999). Innovative hollow fiber ceramic membranes. *American Ceramic Society Bulletin*, *78*(12), 51–55.

Civan, F. (1998). Practical model for compressive cake filtration including fine particle invasion. *A.I.Ch.E. Journal*, *44*, 2388–2398.

Darcovich, K., & Cloutier, C. R. (1999). Processing of functionally gradient ceramic membrane substrates for enhanced porosity. *Journal of the American Ceramic Society*, *82*, 2073–2079.

Davis, R. H., & Hassen, M. A. (1988). Spreading of the interface at the top of a slightly polydisperse sedimenting suspension. *Journal of Fluid Mechanics*, *196*, 107–134.

Hampton, J. H. D., Savage, S. B., & Drew, R. A. L. (1992). Experimental analysis of fine-particle migration during ceramic filtration processes. *Journal of the American Ceramic Society*, *75*, 2726–2732.

Kynch, G. J. (1952). A theory of sedimentation. *Transactions of the Faraday Society*, *48*, 166–176.

Masliyah, J. H. (1979). Hindered settling in a multi-species particle system. *Chemical Engineering Science*, *34*, 1166–1168.

Nijmeijer, A., Huiskes, C., Sibelt, N. G. M., Kruidhof, H., & Verweij, H. (1998). Centrifugal casting of tubular membrane supports. *American Ceramic Society Bulletin*, *77*(4), 95–98.

Patwardhan, V. S., & Tien, C. (1985). Sedimentation and liquid fluidization of solid particles of different sizes and densities. *Chemical Engineering Science*, *40*, 1051–1060.

Philipse, A. P. (1997). Colloidal sedimentation (and filtration). *Current Opinion in Colloid & Interface Science*, *2*, 200–206.

Schwalbe, D., Kooijman, H. A., & Taylor, R. (1996). Solving Stiff Differential Equations and Differential Algebraic Systems with Maple V. *Maple Technology*, *3*, 47–53.

Yu, A. B., & Standish, N. (1987). Porosity calculation of multicomponent mixtures of spherical particles. *Powder Technology*, *52*, 233–241.